

# A Rapid Synthesis of Oriented Palladium Nanoparticles by UV Irradiation

S. Navaladian · B. Viswanathan ·  
T. K. Varadarajan · R. P. Viswanath

Received: 28 August 2008 / Accepted: 20 November 2008 / Published online: 4 December 2008  
© to the authors 2008

**Abstract** Palladium nanoparticles of average size around 8 nm have been synthesized rapidly by UV irradiation of mixture of palladium chloride and potassium oxalate solutions. A rod-shaped palladium oxalate complex has been observed as an intermediate. In the absence of potassium oxalate, no Pd nanoparticles have been observed. The synthesized Pd nanoparticles have been characterized by powder X-ray diffraction (XRD), transmission electron microscopy (TEM), selective area electron diffraction and energy dispersive analysis by X-rays (EDAX) analyses. XRD analysis indicates the preferential orientation of catalytically active {111} planes in Pd nanoparticles. A plausible mechanism has been proposed for the formation of anisotropic Pd nanoparticles.

**Keywords** Pd nanoparticles · UV irradiation · Potassium oxalate · Preferential orientation · Texture coefficient

## Introduction

Nanoparticles of noble metals are gaining importance because of their applications in various fields as well as their considerable stability. Palladium nanostructures have been known as hydrogen sensors [1] and catalysts for the reactions such as oxidation of hydrocarbon in automobiles (three-way catalyst) [2], hydrogenation [3], Heck reaction [4], Suzuki

reaction [5], Stille coupling [6] and C–N coupling [7]. Also, Pd nanoparticles with preferentially exposed {111} show high catalytic activity for the hydrogenation of 1,3-butadiene. Several synthetic methods have been reported regarding the preparation of stable palladium nanoparticles. Some of the methods are sonochemical [8],  $\gamma$ -irradiation [9], UV irradiation [10], microemulsion technique [11] and polyol reduction [12]. However, the facile, cost-effective and large-scale synthetic methods are still elusive. Herein, we report a simple, rapid, surfactantless and room temperature synthesis of Pd nanoparticles by UV irradiation of the mixture of PdCl<sub>2</sub> and K<sub>2</sub>C<sub>2</sub>O<sub>4</sub> solutions.

## Experimental

In a typical synthesis, a mixture of 20 mL of 5 mM PdCl<sub>2</sub> (Sigma-Aldrich, 99.9% purity) solution and 20 mL of 25 mM K<sub>2</sub>C<sub>2</sub>O<sub>4</sub> (Merck, 99% purity) solution were stirred for 5 min. Formation of reddish yellow needles was observed. But, upon further dilution, the needles disappeared. Nitrogen gas was purged through reaction mixture for 5 min. Then, the mixture in a quartz tube was irradiated using 450 W Hg lamp (Oriental Corporation, USA) for 5 min in order to get the black precipitate. No cut-off filters have been used. Upon irradiation, orange coloured solution turned to colourless and particles formed settled down due to the self-assembly caused by oxalate di anion. The black particles were washed with distilled water by centrifugation at 6000 rpm.

## Characterization

The synthesized Pd nanoparticles were characterized by powder X-ray diffraction (XRD), transmission electron

S. Navaladian · B. Viswanathan · T. K. Varadarajan ·  
R. P. Viswanath (✉)  
Department of Chemistry, National Centre for Catalysis  
Research, Indian Institute of Technology Madras,  
Chennai 600 036, India  
e-mail: rpv@iitm.ac.in

microscopy (TEM), selective area electron diffraction (SAED) and energy dispersive analysis by X-rays (EDAX). Powder XRD patterns of samples were recorded with a SHIMADZU XD-D1 diffractometer using Ni-filtered  $\text{CuK}_\alpha$  radiation ( $\lambda = 1.5406 \text{ \AA}$ ) with the scan rate of  $0.1^\circ/\text{s}$ . TEM analysis was carried out using a Philips CM12 TEM working at a 100 kV accelerating voltage. Samples for TEM analysis were prepared by dispersing Pd nanoparticles in ethanol followed by drop-casting on a copper grid (400 mesh) coated with carbon film.

## Results and Discussion

TEM images of black particles are shown in Fig. 1a and b. Aggregates of irregular-shaped particles are observed and the size of Pd particles varies from 8 to 25 nm. A nanorod also is observed in TEM image as shown in Fig. 1a. The aggregates of particles are formed due to the self-assembling nature of oxalate di anion. This self-assembly of the particles also confirms the capping ability of oxalate on Pd surface. Hence, it was difficult to calculate the particle size distribution from TEM images. SAED given in Fig. 1c shows a ring pattern. Those rings are indexed to be

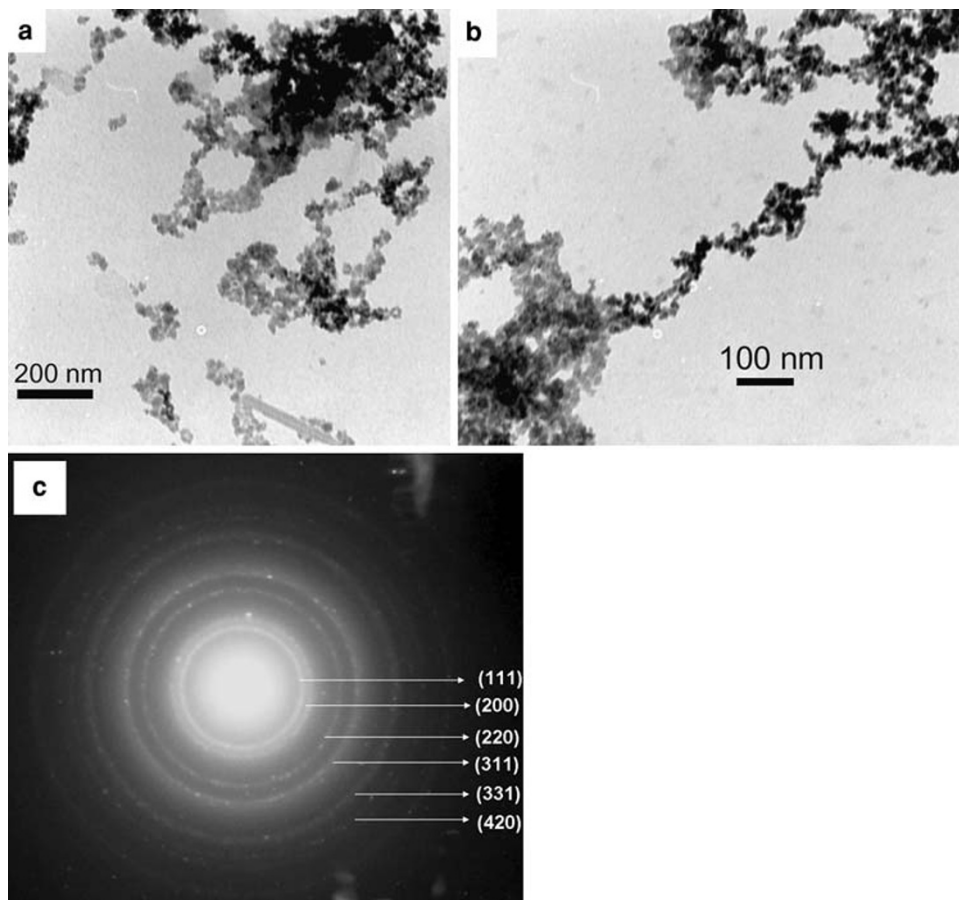
corresponding to (111), (200), (220), (311), (331) and (420) of Pd metal with fcc structure (JCPDS file no. 87-0638).

Powder XRD pattern of Pd nanoparticles is shown in Fig. 2. The  $d$ -spacing corresponding to XRD lines are 2.236, 1.936, 1.369, 1.170 and 1.116  $\text{\AA}$ . These  $d$ -spacing values correspond to (111), (200), (220), (311) and (222) planes with lattice constant,  $a = 3.871 \text{ \AA}$ , matching with that of JCPDS file 87-0638. This observation confirms the presence of metallic Pd with fcc structure. XRD line corresponding to {111} plane is found to be unusually intense. In order to understand the preferential orientation of crystal planes, the average crystallite size of the Pd nanoparticles has been calculated using Scherer equation, and texture coefficient has been calculated [13] by Halls method from the each line in XRD powder pattern of Pd nanoparticles. The texture coefficient ( $C_{hkl}$ ) has been calculated using Eq. 1 [14].

$$C_{(hkl)} = \frac{I_{(hkl)i}}{I_{o(hkl)i}} / \frac{1}{n} \sum_n \frac{I_{(hkl)n}}{I_{o(hkl)n}}, \quad (1)$$

where  $C_{(hkl)}$  is the texture coefficient of the facet  $\{hkl\}$ ,  $I_{(hkl)}$  is the intensity of the  $(hkl)$  reflection of the sample under analysis,  $I_{o(hkl)}$  is the intensity of the  $(hkl)$  reflection of a polycrystalline bulk sample and ‘ $n$ ’ is the number of

**Fig. 1** a, b TEM images of Pd nanoparticles synthesized by photochemical decomposition method; c SAED pattern recorded on aggregates of Pd nanoparticles



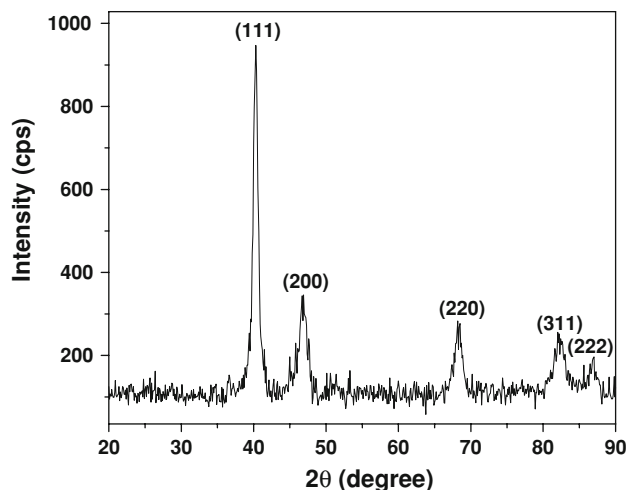


**Fig. 2** XRD powder pattern of Pd nanoparticles

reflections taken into account. By using this equation, the preferential orientation of the facets can be understood.  $C_{(hkl)}$  is expected to be unity for the facet, which does not have preferential orientation. If it is higher than unity, it is a preferentially grown facet.  $C_{(hkl)}$  values and average crystallite sizes of different facets of the Pd nanoparticles are shown in Fig. 3. For calculating texture coefficient, JCPDS file 87-0639 of Pd has been used. Average crystallite size corresponding to the various crystal planes of Pd nanoparticles differs from 6.5 to 11.5 nm. It is clear from the plot that the average crystallite sizes pertaining to (111) and (222) reflections are higher than that of the other planes. This indicates the preferential orientation of {111} facet in Pd nanoparticles [15]. This reveals that particles are anisotropic in shape (non-spherical). The average crystallite size calculated from XRD pattern is less than that of from TEM. This implies the polycrystalline nature of the Pd nanoparticles. In general, for the spherical

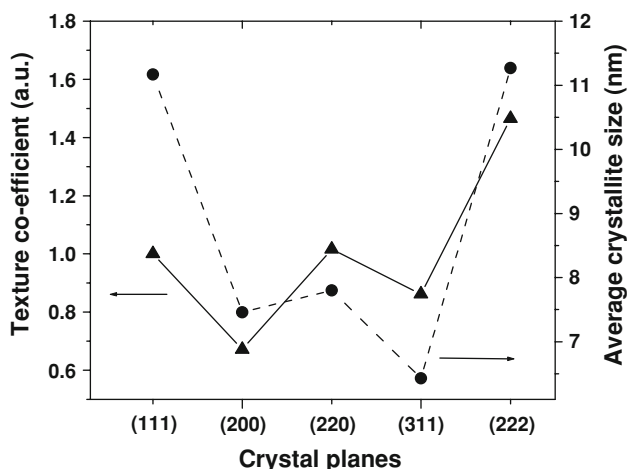


**Fig. 3** Average crystallite size and texture coefficient of Pd nanoparticles calculated from XRD powder pattern

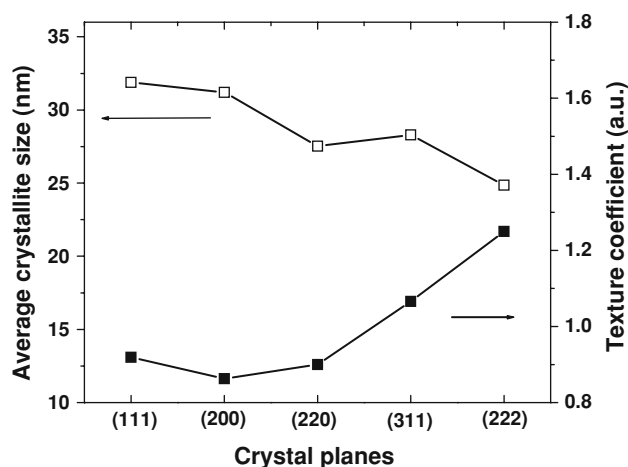
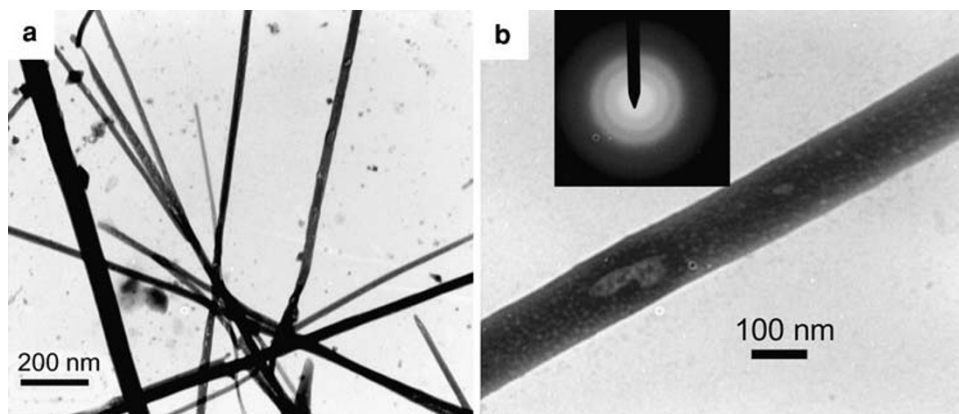


**Fig. 4** Average crystallite size and texture coefficient of spherical Ag nanoparticles calculated from XRD powder pattern (reference JCPDS file used for the calculation is 89-3722)

particles, average crystallite size of crystal planes is expected to decrease while moving from lower to higher Bragg angle [16]. For the comparison, the average crystallite size and texture coefficient calculated from the XRD powder pattern of spherical Ag nanoparticles [17] of size around 30 nm are given in Fig. 4. The expected trend is observed in the average crystallite size for various crystal planes in the case of Ag nanospheres.

In the plot of the texture coefficients, the similar deviation among the texture coefficients of various facets is observed for Pd nanoparticles. But in the case of texture coefficient of Ag nanospheres given in Fig. 5, texture coefficient of various crystal planes is found to increase while moving from lower to higher Bragg angle. In the case of (111), texture coefficient is found to be around 1. But in the case of (222) plane, the texture coefficient is around 1.4. Even though (111) and (222) are parallel planes, there is a great deviation between their texture coefficients. This implies that even though the morphology is spherical, the texture coefficient varies between polycrystalline bulk sample and nanoparticles. In the case of nanoparticles, the planes of higher Bragg angles show more intensity than that of lower Bragg angles. This deviation is expected mainly due to the effect of particle size in X-ray scattering. The scattering of X-rays by nanoparticles and polycrystalline bulk sample is different. Similar phenomenon is observed in another report where peak of (222) is highly intense than that of (111) [18]. Due to the unusual high intensity of higher angle peaks of (220), (311) and (222) planes in the case of Pd nanoparticles, the intensity of (111) planes is observed to be less. However, the deviation in texture coefficient values in the case of Pd nanoparticles reveals the anisotropic shape of Pd nanoparticles with preferential orientation of {111} facet.

**Fig. 5** TEM image of intermediate complex,  $K_2[Pd(C_2O_4)_2]$ . Inset of (b) shows the SAED pattern of the nanorod



TEM images of the intermediate reddish yellow needles formed before irradiation are given Fig. 5a and b. TEM image (Fig. 5a) shows the wire-like morphology. Thickness of the rods varies from 15 to 80 nm and the length is more than 1  $\mu$ m. Figure 5b shows the surface of a single rod of thickness 125 nm. SAED pattern in Fig. 5b shows the rings revealing the polycrystalline nature of the rod-shaped intermediate complex. Since the needles are visible to eyes, it is evident that a wide range of sizes of needles of the intermediate complex is possible. The corresponding EDAX spectrum is shown in Fig. 6. EDAX spectrum shows the presence of K, Pd, Cu, C and O. Cu and C come from a carbon-coated copper grid used for TEM analysis. These observations indicate the formation of a water soluble,  $K_2[Pd(C_2O_4)_2]$ , complex. As per the literature, this complex can be synthesized by the reaction of  $Pd(OH)_2$  and oxalic acid [19]. In the case of Pt also, a similar kind of oxalate complex with the wire morphology has been observed [20]. In the absence of oxalate, irradiation of  $PdCl_2$  solution has not yielded any Pd nanoparticles even after 30 min of UV irradiation.

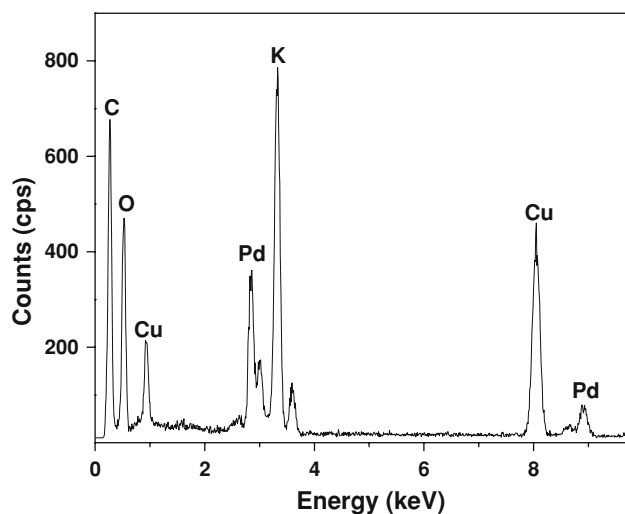
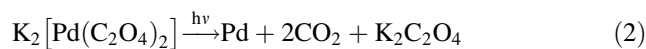


**Fig. 6** EDAX spectrum of intermediate complex,  $K_2[Pd(C_2O_4)_2]$

In the case of UV irradiation method using  $PdCl_2$  and 2-propanol (reducing agent), it needs around 24 h to form Pd nanoparticles [10]. This is due to the poor reducing ability of 2-propanol. In the case of Triton X-100 as reducing agent, UV irradiation for 30 min is required for the formation of Pd nanoparticles [21]. But, in the current procedure, reduction of Pd by oxalate occurs so rapidly and 5 min of UV irradiation is sufficient for the complete reduction of  $PdCl_2$  (20 mL of 5 mM) to Pd nanoparticles. High reducing ability and photosensitivity of oxalate di anions are responsible for the rapid decomposition [22]. Since the standard reduction potentials of Pd ( $E^0(Pd^{2+}/Pd) = 0.951$  V) [23] and oxalate di anion ( $E^0(2CO_2/C_2O_4^{2-}) = -0.49$  V) [20] are favourable, decomposition occurs rapidly under UV irradiation to yield metallic Pd as shown in Eq. 2.



Also, mere refluxing of  $PdCl_2$  and potassium oxalate solution has not yielded any Pd nanoparticles even after 30 min. This observation reveals the importance of UV light for this decomposition reaction to occur for yielding metallic Pd. It is worthwhile to mention that more the intensity of the lamp more will be the conversion. Hence, in the current method, a high intensity lamp was utilized to synthesize Pd nanoparticles rapidly. Mechanism of decomposition of  $[Pd(C_2O_4)_2]^{2-}$  is similar to that of silver oxalate ( $Ag_2C_2O_4$ ) [22]. It is because decomposition of  $Ag_2C_2O_4$  under UV light is also so rapid. Decomposition of  $Ag_2C_2O_4$  is well explored in the literature [22]. Hence, mechanism of decomposition of  $[Pd(C_2O_4)_2]^{2-}$  can be explained as follows. In this reaction, oxalate di anion in the intermediate complex,  $[Pd(C_2O_4)_2]^{2-}$ , absorbs the light in the UV region [24], get excited and decomposes to  $CO_2$ . During the decomposition, electrons are transferred simultaneously to  $Pd^{2+}$ . Thus, the reduction of  $Pd^{2+}$  ions to yield Pd metal occurs. In general, this phenomenon is known as photo redox-decomposition [25]. Formation of  $CO_2$  has been confirmed by the formation of white

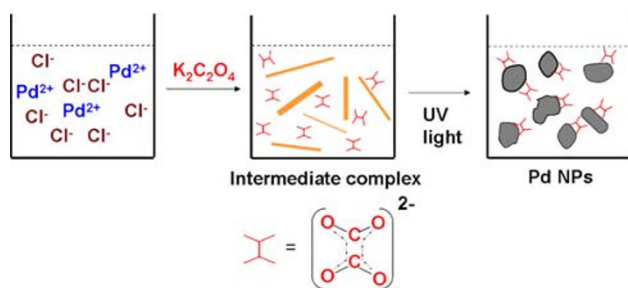


**Fig. 7** Schematic representation of the formation of Pd nanoparticles by the photochemical decomposition method

precipitate (BaCO<sub>3</sub>) observed when the outlet of the reaction was dipped in Ba(OH)<sub>2</sub> (baryta) solution [26].

Even though powerful capping agents such as poly (vinyl pyrrolidone) have not been employed in this method, formation of Pd nanoparticles has been observed. This is expected due to the fast nucleation and particle growth of Pd. Pd atoms are generated during the photochemical decomposition and nucleation starts immediately after attaining certain concentration (saturation) of Pd atoms. The nuclei further grow into the particle. In the current synthesis, generation of Pd atoms is so rapid and therefore the nucleation as well as particle growth is faster. Hence, possibility for the homogenous nucleation is high. As a result, number of nuclei formed is so high and hence, particle size is small. Moreover, there is a chance for the simultaneous agglomeration and the explosion of metal nanoparticles into small clusters in the presence of UV light [27–29]. Faceting of the crystals may occur due to the selective adsorption of oxalate di anion on certain planes of Pd nuclei. As a result, uncapped planes of the nuclei tend to grow with higher rates and give rise to the formation of anisotropic (non-spherical) nanoparticles of Pd [20]. In this case, K<sup>+</sup> does not have any specific role in the resulting morphology of metal nanoparticles, because K<sup>+</sup> does not adsorb on metal nuclei to influence the morphology in the synthesis of metal nanoparticles [30]. Synthesis of Pd nanoparticles from PdCl<sub>2</sub> and potassium oxalate is schematically explained in Fig. 7. The optimized geometry of oxalate di anion is shown in the schematic mechanism [31].

## Conclusions

Anisotropic palladium nanoparticles can be synthesized rapidly by the UV irradiation of mixture of PdCl<sub>2</sub> and potassium oxalate solutions without any surfactant or polymer capping agents. The intermediate oxalatopalladium(II) complex exhibits a rod-like morphology. The formation of nanoparticles occurs rapidly at room temperature, in the presence of UV light, due to the favourable

reducing ability of the oxalate. The resulting {111}-oriented Pd anisotropic nanoparticles are expected to have promising catalytic activity for various reactions. This facile synthetic protocol can be exploited in the preparation of supported Pd catalysts for various reactions.

**Acknowledgement** The authors wish to thank CSIR, New Delhi, for the financial assistance.

## References

- M.Z. Atashbar, S. Singamaneni, *Sens. Actuators. B Chem.* **111–112**, 13 (2005). doi:10.1016/j.snb.2005.07.034
- Y. Nishihata, J. Mizuki, T. Akao, H. Tanaka, M. Uenishi, M. Kimura, T. Okamoto, N. Hamadak, *Nature* **418**, 164 (2002). doi:10.1038/nature00893
- J.S. Albero, G. Rupprechter, H.J. Freund, *J. Catal.* **235**, 52 (2005)
- C. Vincenzo, N. Angelo, M. Antonio, D. Antonia, I. Patrizia, *Organometallics* **22**, 4193 (2003). doi:10.1021/om034020w
- Y. Li, E. Boone, M.A. El-Sayed (2002) *Langmuir* **18**, 4921. doi:10.1021/la011469q
- J.C.G. Martinez, R. Lezutekong, R.M. Crooks, *J. Am. Chem. Soc.* **127**, 5097 (2005). doi:10.1021/ja042479r
- V. Kogan, Z. Aizenshtat, R. Popovitz-Biro, R. Neumann, *Org. Lett.* **4**, 3529 (2002). doi:10.1021/ol026689p
- N.A. Dhas, A. Gedanken, *J. Mater. Chem.* **8**, 445 (1998). doi:10.1039/a706100e
- A.A. Athawale, S.V. Bhagwat, P.P. Katre, A.J. Chandwadkar, P. Karandikar, *Mater. Lett.* **57**, 3889 (2003). doi:10.1016/S0167-577X(03)00235-0
- C.Y. Wang, Y. Zhou, Z.Y. Chen, Q.Y. Lu, X. Mo, *J. Nanopart. Res.* **1**, 479 (1999)
- M. Iida, S. Ohkawa, H. Er, N. Asaoka, H. Yoshikawa, *Chem. Lett.* **10**, 1050 (2002). doi:10.1246/cl.2002.1050
- Y. Xiong, J.M. McLellan, J. Chen, Y. Yin, Z.Y. Li, Y. Xia, *J. Am. Chem. Soc.* **127**, 17118 (2005). doi:10.1021/ja056498s
- B. Cullity, *Elements of X-ray Diffraction* (Addison-Wesley, Reading, MA, 1987)
- S. Karim, M.E. Toimil-Molares, F. Maurer, M.W. Ensinger, J. Liu, T.W. Cornelius, R. Neumann, *Appl. Phys. A* **84**, 403 (2006). doi:10.1007/s00339-006-3645-6
- M.K. Aminian, N. Taghavinia, A. Irajizad, S.M. Mahdavi, M. Chavoshi, S. Ahmadian, *Nanotechnology* **17**, 520 (2006). doi:10.1088/0957-4484/17/2/030
- A.R. West, *Solid State Chemistry and Its Applications* (Wiley, New York, 1998)
- S. Navaladian, *Strategies for the synthesis of nanomaterials*. Ph.D. Thesis, Indian Institute of Technology Madras, 2008
- H. Wang, D.O. Northwood, *Res. Lett. Mater. Sci.* **2008**, 619032 (2008)
- M.L. Blokhina, A.I. Blokhin, M.Ya. Nikulin, M.G. Derikova, *Powder Metal. Metab. Ceram.* **35**, 3 (1996)
- S. Navaladian, C.M. Janet, B. Viswanathan, T.K. Varadarajan, R.P. Viswanath, *J. Phys. Chem. C* **111**, 14150 (2007). doi:10.1021/jp0744782
- S. Nath, S. Praharaj, S. Panigrahi, S. Basu, T. Pal, *Curr. Sci.* **786**, 92 (2007)
- V.V. Boldyrev, *Thermol Chim. Acta.* **388**, 63 (2002)
- G. Milazzo, S. Caroli, V.K. Sharma, *Tables of Standard Electrode Potentials* (Wiley, New York, 1978)
- S. Dey, P. Banerjee, S. Gangopadhyay, P. Vojtisek, *Transit Met. Chem.* **28**, 765 (2003). doi:10.1023/A:1026073108597

25. W. Adamson, *Pure Appl. Chem.* **20**, 25 (1969). doi:[10.1351/pac196920010025](https://doi.org/10.1351/pac196920010025)
26. S. Navaladian, B. Viswanathan, R.P. Viswanath, T.K. Varadarajan, *Nanoscale Res. Lett.* **2**, 44 (2007). doi:[10.1007/s11671-006-9028-2](https://doi.org/10.1007/s11671-006-9028-2)
27. H. Fujiwara, S. Yanagida, P.V. Kamat, *J. Phys. Chem. B* **103**, 2589 (1999). doi:[10.1021/jp984429c](https://doi.org/10.1021/jp984429c)
28. A. Takami, H. Kurita, S. Koda, *J. Phys. Chem. B* **103**, 1226 (1999). doi:[10.1021/jp983503o](https://doi.org/10.1021/jp983503o)
29. S. Link, Z.L. Wang, M.A. El-Sayed, *J. Phys. Chem. B* **104**, 7867 (2000). doi:[10.1021/jp0011701](https://doi.org/10.1021/jp0011701)
30. A. Filankembo, S. Giorgio, I. Lisiecki, M.P. Pileni, *J. Phys. Chem. B* **107**, 7492 (2003). doi:[10.1021/jp022282q](https://doi.org/10.1021/jp022282q)
31. F.A. Cotton, C.Y. Liu, C.A. Murillo, D. Villagran, X. Wang, *J. Am. Chem. Soc.* **125**, 13564 (2003). doi:[10.1021/ja036884e](https://doi.org/10.1021/ja036884e)